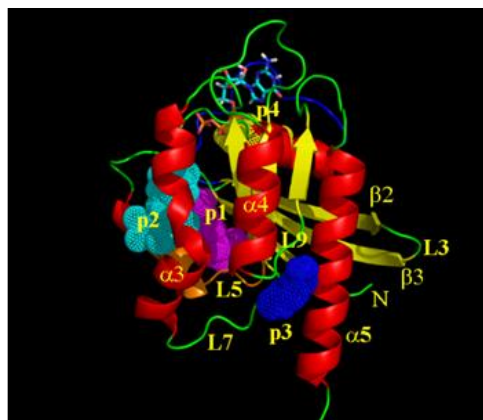
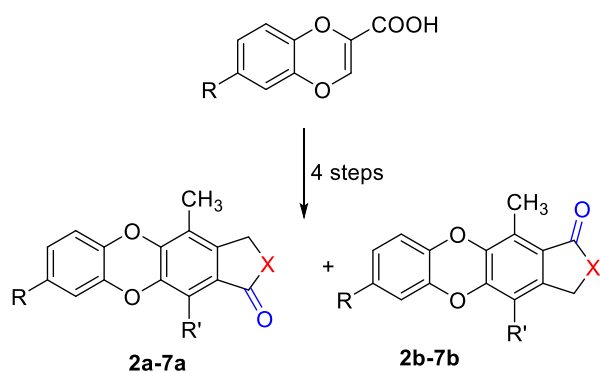


Graphical Abstract:

Multigram scale synthesis of polycyclic lactones and evaluation of antitumor and other biological properties

Laura Grau, Manel Romero, Cristian Privat-Contreras, Daniela Presa, Miquel Viñas, Jordi Morral, Klaus Pors,* Jaime Rubio-Martinez,* and M. Dolors Pujol*



Highlights

- A series of polycyclic lactones containing 1,4-dioxine core was synthesized.
- The series **a** exhibited KRasWnt inhibition while the **b** series was inactive.
- Lactone **2a** presents the best KRas activity profile on SW480 cell type.
- Molecular modeling studies showed that compound **2a** was inserted in KRas protein.

Multigram scale synthesis of polycyclic lactones and evaluation of antitumor and other biological properties

Laura Grau,[‡] Manel Romero,[‡] Cristian Privat-Contreras,[#] Daniela Presa,[§] Miquel Viñas,[‡] Jordi Morral,[§] Klaus Pors^{§*} Jaime Rubio-Martinez,^{#*} and Maria Dolors Pujol^{‡*}

[‡]*Laboratori de Química Farmacèutica (Unitat Associada al CSIC). Facultat de Farmàcia. Universitat de Barcelona. Av. Joan XXIII, 27-31. E-08028-Barcelona, Spain*

[§]*Institute of Cancer Therapeutics, School of Pharmacy and Medical Sciences, Faculty of Life Sciences, University of Bradford. BD7 1DP, West Yorkshire, U.K.*

[#]*Department of Physical Chemistry, Faculty of Chemistry, University of Barcelona and the Institute de Recerca en Química Teòrica i Computacional (IQTCUB), E-08028-Barcelona, Spain*

Keywords: ellipticine, 1,4-benzodioxine derivatives, tetracyclic lactones, antitumor compounds

Abstract. An efficient four-step synthesis of tetracyclic lactones from 1,4-benzodioxine-2-carboxylic acid was developed. Ellipticine derivatives exhibit antitumor activity however only a few derivatives without carbazole subunit have been studied to date. Herein, several tetracyclic lactones were synthesized and biologically evaluated. Several compounds (**2a**, **3a**, **4a** and **5a**) were found to be inhibitors of the Kras-Wnt pathway. The lactone **2a** also exerted a potent inhibition of Tau protein translation and was shown to have capacity for CYP1A1-bioactivation. The results obtained are further evidence of the therapeutic potential of tetracyclic lactones related to ellipticine. Molecular modeling studies showed that compound **2a** is inserted between helix α 3 and α 4 of the KRas protein making interactions with the hydrophobic residues Phe90, Glu91, Ile9364, Hie94, Leu133 and Tyr137 and a hydrogen bond with residue Arg97.

1. Introduction

Ellipticine (5,11-dimethyl-6*H*-pyrido[4,3-*b*]carbazole, **1**), is a planar tetracyclic alkaloid that presents an interesting cytotoxic activity attributable to multiple mechanisms of action. However, the therapeutic applications of ellipticine remain limited because of the large number of side effects [1]. Interest in the ellipticine pharmacophore has attracted the attention of many research groups because of their multiple biological activities [2] and especially for their capacity to inhibit cancer cell growth [3].

Previously, we have reported on ellipticine derivatives in which the indole nucleus has been replaced by 1,4-benzodioxine as interesting bioactive compounds, but their mechanism of action was not confirmed [4]. In this study, we report the preparation of ellipticine derivatives containing the 1,4-benzodioxine nucleus and a lactone replacing the pyridine system. These structural changes and the presence of different substituents make these compounds interesting and promising antitumor candidates.

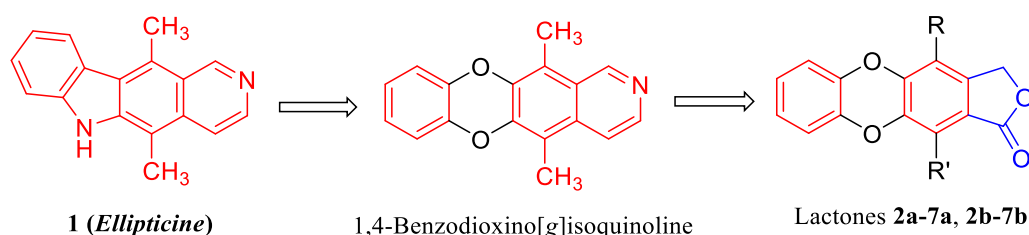


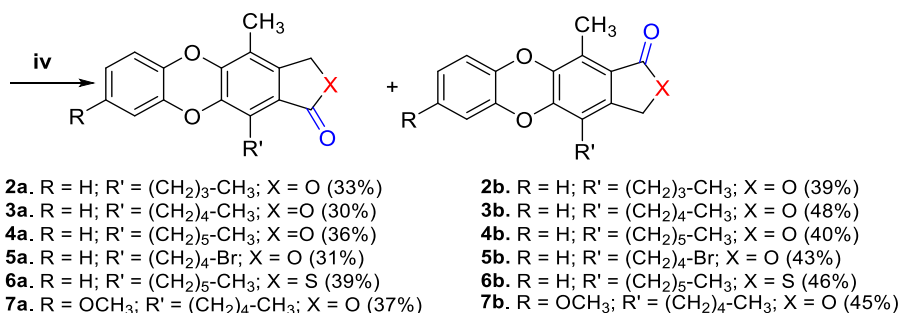
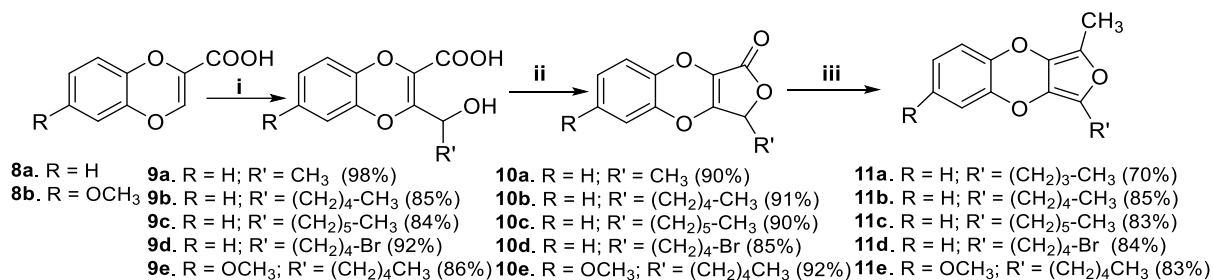
Figure 1. *Ellipticine* and analogues

Compounds containing a 1,4-benzodioxine subunit have received significant attention as a useful scaffold in chemical and pharmaceutical research. The lactones **2a-7a** and **2b-7b** were prepared in four steps from 1,4-benzodioxin-6-carboxylic acids using previously published methodology to prepare small quantities for biological investigations [5]. In this work, we have refined the methodology to enable multigram scale synthesis (Scheme 1) and reported on the antiproliferative activity of these compounds and investigations to understand their mechanism of action including KRas/Wnt inhibition, angiogenesis inhibition and cytochrome P450 1A1 (CYP1A1) bioactivation.

2. Results and discussion

2.1. Chemistry

Carboxylic acids **8a-b**, hydroxyacids **9a-e**, tricyclic lactones **10a-e** and substituted dienes **11a-e** were prepared on a gram scale by the procedures previously described by us without major changes [5]. The yields with which these compounds were obtained are indicated in Scheme 1 and are practically in the same order as those reported. Then the last stage involves Diels-Alder condensation of the dienes **11a-e** with 2(5*H*)-furanone catalysed by BF₃.Et₂O that leads to a mixture of tetracyclic lactones **a** and **b** depending on the position of the carbonyl group regarding the long alkyl side chain (R'). Both positional isomers (**2a-7a** and **2b-7b**) were separated by column chromatography. Likewise lactones **6a-b** were obtained by Diels-Alder cycloaddition of the diene **11c** and the 2(5*H*)-thiofuranone following the same Diels-Alder methodology. In this work the amount of 2(5*H*)-furanone or 2(5*H*)-thiofuranone added doubled, the amount of solvent was reduced and the reaction time was lengthened compared to the first work described [5]. With these changes, the yields of both isomers are significantly increased (for **2a**, the yield has increased from 20 to 33% and for **2b** from 24 to 39%; **3a** had an improvement of 19 to 30% and **3b** of 25 to 48%; **4a** of 21 to 36% and **4b** of 25 to 40%; **5a** of 19 to 31% and **5b** of 23 to 43%; **6a** was obtained in 20% and now in 39% and **6b** has passed from 22 to 46%; **7a** had an improvement of 22 to 37% and **7b** of 24 to 45%). The structures of the prepared compounds are supported by ¹H and ¹³C NMR spectra.



Reagents and conditions: **i:** 1) LDA/THF, 2) R'CHO. **ii:** PTSA/toluene. **iii:** 1) Li-CH₃, (CH₃)₃SiCl, 2) NH₄Cl. **iv:** 2(5*H*)-furanone or 2(5*H*)-thiofuranone /BF₃·Et₂O

Scheme 1. Synthesis of tetracyclic lactones

2.2. Biological activity profiling. All the title compounds **2a-7a** and **2b-7b** were subjected to biological tests. While many ellipticine analogues exert anticancer activity by inhibition of topoisomerase I and/or II it appears that tetracyclic lactone congeners do not target these enzymes or DNA for antiproliferative activity [5]. To study the biological properties we collaborated with Eli Lilly laboratories within the OIDD program [6] and the results are shown in Tables 1-5.

2.2.1. KRas Inhibition. KRas mutations are involved in the development of many human tumors. Progression to colorectal cancers (CRC) requires a second event such as an activating KRas mutation, which is triggered by undefined interactions between the Wnt signalling pathways and the KRas protein [7]. The KRas synthetic lethal phenotypic assay measures survival of CRC cells carrying mutations that activate both Wnt and KRas signaling relative to those with other driver mutations [7]. The measurement of ATP is an accepted method to estimate the number of viable cells. Human CRC cell lines with KRas mutations (DLD-1, HCT116, and SW480) were used to test the effect of the tetracyclic lactones on cell proliferation *in vitro* [8].

The results showed that compounds **2a**, **3a**, **4a** and **5a** exerted dose-dependent inhibition of CRC cells while compounds **2b**, **3b**, **4b**, **5b**, **6b**, and **7b** generally were less potent active (see Table 1). Interestingly, a limited inhibitory effect was observed at the lowest dose of **2a** in HCT116 cells, but it increased substantially in glycogen synthase kinase-3 GSK3- β inhibitor HCT pretreated cells. This result indicates an effect on the Wnt pathway at low dose (0.2 μ M) but not at the higher doses investigated (2 and 20 μ M). The data also reveals that, in general, the compounds presenting the carbonyl group of lactone on the same side as the long alkyl chain (series a) are more potent compounds than when it is on the side of the methyl group (series b) (see position of R', Scheme 1).

Table 1. Basal viability of [1,4]-benzodioxine analogues in a panel of colorectal cancer cells lines using ATP assay

KRAS-Wnt synthetic lethal primary single point assay													
CRC cell type	[μ M] test	2a % inh.	2b % inh.	3a % inh.	3b % inh.	4a % inh.	4b % inh.	5a % inh.	5b % inh.	6a % inh.	6b % inh.	7a % inh.	7b % inh.
SW480	0.2	17	12	20	11	21	16	7	-40	13	10	15	
	2	73	14	64	21	58	18	62	4.4	9	10	16	
	20	138	14	86	40	86	12	63	55	22	21	19	-10.7
DLD-1	0.2	17	-29	60	-11	14	29	30	0.4	-9	-10	-17	
	2	65	6	63	17	50	49	45	0.4	7	6	16	
	20	91	41	120	40	112	-15	76	20	90	14	73	-3.9
HCT116	0.2	5	39	20	-9	12	-3	33	2	-17	-10	-14	
	2	66	7	62	12	60	7	56	9.5	10	2.9	7.9	
	20	78	38	89	35	91	15	76	108	40	13	40	26
HCT116 GSK3- β inhibitor pretreated	0.2	67	-58	5	44	52	26	15	12	-29	-106	52	
	2	63	0.4	59	28	69	10	58	20	-4	-5.6	8	
	20	80	2	66	31	62	2	53	28	18	3.4	6	

The length of alkyl chain (4, 5 or 6 carbons (**2a**, **3a** and **4a**)) modifies cytotoxic activity very little. Likewise, the introduction of halogen on the alkyl chain (**5a**) produces only slight modifications in the activity, while the change from lactone to thiolactone leads to a pronounced decrease in potency (**6a** and **6b**). Finally, the introduction of a methoxyl group as a substituent of the first aromatic ring of the

tetracyclic lactone (at the C-7 position) also produces a marked loss in cytotoxicity (**7a** and **7b**) attributable to that the substituent difficult the binding to the active site of the target.

2.2.2. Angiogenesis inhibition. Angiogenesis and vasculogenesis facilitates blood vessel sprouting and tube formation, processes which can be modified using vascular disrupting agents (VDAs) that cause rapid collapse and shut down of established cancer blood vessels leading to regional tumor ischemia and necrosis [9]. Often inhibitors of angiogenesis bind the extracellular domain of vascular endothelial growth factor (VEGF) receptor-2 [10] or the specialized ligands VEGF-A, VEGF-C and VEGF-D [11]. Monoclonal antibodies targeting endothelial factors have been studied and approved by the FDA for the treatment of several tumors [12]; however, it should be noted that small molecules with the same therapeutic use are still not medically used.

The results showed that compounds **2a**, **3a**, **4a** and **5a** (**a** series) possessed a high antiangiogenic activity on tube area but not on nuclear count, demonstrating selectivity of these compounds, while the compounds in the **b** series (**2b**, **3b**, **4b**, **5b**, **6b**, and **7b**) were inactive in both assays (Table 2). In addition, side alkyl chains with more than 5 C lead to inactive compounds. Compounds (**2a**, **3a**, **4a** and **5a**) could be of interest for the reduction of angiogenesis in endothelial tube formation without causing antiproliferative activity. As observed in the KRas inhibition assay, compounds possessing an alkyl substituent on the same side as the carbonyl group of the lactone were also the most potent analogues as antiangiogenic inhibitors.

Table 2. Antiangiogenic data from endothelial tube and nuclear tests

Comp.	Angio TubeArea (IC₅₀ μM)	Angio NucArea (IC₅₀ μM)
2a	1.5±0.2	>10
2b	-	-
3a	1.3±0.1	>10
3b	>10	>10
4a	1.0±0.2	>10

4b	-	-
5a	0.7±0.2	>10
5b	>10	>10
6a	>10	>10
6b	inactive	inactive
7a	inactive	inactive
7b	inactive	inactive

2.2.3. Cellular Cycle Phase. In general, the timing of key cell-cycle phase transitions is controlled by cell-cycle checkpoints, which prevent cells from advancing inappropriately or prematurely to the next phase of the cell cycle. A particularly critical checkpoint occurs in G2/M and governs cellular commitment to enter cytokinesis. The results suggests that compounds **2a**, **3a**, **4a** and **5a** have an effect on cell cycle progression of HeLa cells on 2N, 4N and MI due to arrest of cells (Table 3), while compounds **6a** and **7a** showed no activity at the concentrations tested. All **b** isomers were also inactive.

Table 3. Cellular Cycle Phase on Hela

Comp.	Hela CellCyc	Hela cellCyc	Hela CellCyc	Hela CellCyc	G1 arrest	S Phase
	2N (IC₅₀ μM)	4N (EC₅₀ μM)	MI (EC₅₀ μM)	Num (IC₅₀ μM)	(EC₅₀ μM)	(IC₅₀ μM)
2a	2.2±0.3	2.0±0.1	2.1±0.1	1.7±0.2	>10	>10
3a	1.8±0.2	1.6±0.3	1.4±0.1	1.0±0.2	>10	>10
4a	2.1±0.1	2.0±0.1	>10	1.8±0.3	>10	>10
5a	1.5±0.1	1.4±0.1	1.3±0.2	0.6±0.2	>10	>10
6a	>10	>10	>10	>10	>10	>10
7a	>10	>10	>10	-	>10	>10
7b	>10	>10	>10	-	>10	>10

It is worthy of note that compounds **7a** and **7b** containing a methoxy group on the aromatic ring are surprisingly inactive in several cytotoxic tests while the methoxylated derivatives of ellipticine showed high cytotoxicity [13].

2.2.4. Wnt pathway activation. Osteoporosis is a silent disease that weakens the bones over time and increases the risks of fractures. The mechanism of bone loss is not yet well understood, but the disorder arises from an imbalance in the formation of new healthy bones and the decrease and resorption of bone tissue. The imbalance is partly triggered by a decrease of bone protein matrix and mineral content [14a]. The aim of a Wnt pathway activator is to discover compounds to increase bone development and especially slow down osteoporosis. In this regard, a phenotypic bone formation assay is useful to evaluate compounds for their ability to differentiate murine C2C12 cells, which possess multi-lineage potential and an osteoblast-like phenotype through β -catenin-dependent stimulation of alkaline phosphatase activity [14b]. Compounds of therapeutic interest increase osteoblast formation in rodent and human cellular assays through a non-glycogen synthase kinase (GSK) mechanism. Tetracyclic lactones **2a**, **3a**, **4a** and **5a** displayed interesting activity by activation of the Wnt pathway through stimulation of alkaline phosphatase activity but not β -catenin (Table 4). The lactones of the series **a** with side chains greater than 5 carbon atoms were practically inactive. The compounds of the **b** series did not show activity either.

Table 4. Wnt pathway activation assay

Comp.	Wnt3a_C2C12	Wnt3a_C2C12
	AlkPhos	β -catenin
	(EC ₅₀ μ M)	(EC ₅₀ μ M)
2a	6.7 \pm 1.9	>20
3a	6.3 \pm 1.5	-
4a	7.6 \pm 1.1	>20

5a	8.2±0.9	>20
6a	>10	>10
7a	>10	>10
7b	>10	>10

2.2.5. Other biological properties [15]. The tau protein is related to neuroprotection and Alzheimer's disease. This protein acts *in vivo* to induce tubulin assembly and stabilize microtubules, and the activity may be necessary but not sufficient for neuronal morphogenesis. Lactone **2a** so do **3a** and **4a** showed important inhibition of Tau protein translation at 40 μ M concentration. In addition, **2a** presents inhibition of other haplotypes such as Angpt18 (inhibit lipoprotein lipase and decrease plasma triglyceride) APOC3 (decrease of triglycerides), Nav1.7 (antinociceptive activity related to sodium ion channel) [15] and PCSK9 (cholesterol-lowering drugs [16]) at 40 μ M (Table 5).

Table 5. Other biological properties evaluated (% inhibition)

Comp.	hTau(40 μM)	hAngpt18(40 μM)	hAPOC3(40 μM)	hNav1.7(40 μM)	hPCSK9(40 μM)
	% inh.	% inh.	% inh.	% inh.	% inh.
2a	92	93	89	76	95
2b	8	15	34	-62	15
3a	88	89	78	74	69
3b	-	-	-	-	-
4a	77	86	75	-25	75
4b	11	24	17	-9	-7
5a	56	67	67	0	35
5b	35	37	17	-32	40
6a	20	31	21	-10	30
6b	30	27	7	-2	-4
7a	60	59	38	22	42
7b	23	34	12	-12	-7

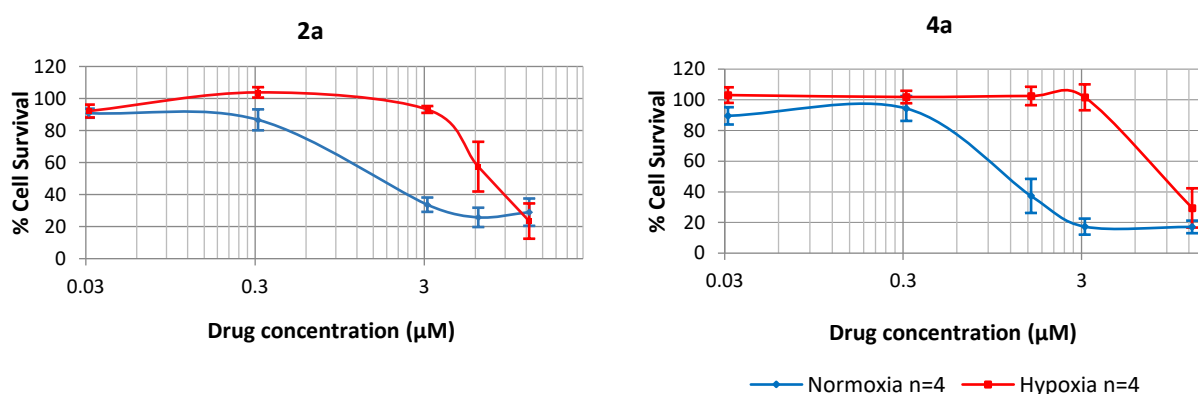
2.2.6. Activity under hypoxic conditions and 3D cell cultures

Solid tumors are often characterized by areas with inadequate blood supply, lower oxygen tension and nutrient supply. Tumor cells distant from the existing blood vascular capillaries ($> 100 \mu\text{m}$) often become hypoxic and resistant to both radio and chemotherapy. It is also known that hypoxia contributes to the progression of a more aggressive phenotype via activation of several genes including induction of hypoxia-inducible factor 1-alpha (HIF1- α) and subsequently VEGF that contributes to angiogenesis [17-20].

As compounds **2a** and **4a** were consistently shown to produce a biological response in all assays investigated and possessed antiangiogenic properties (Table 2), these were selected for interrogation in HT29 colon cancer cells, which harbor wild-type KRas protein, under both normoxic and hypoxic conditions. Both compounds **2a** (HCR = 0.24) and **4a** (HCR = 0.15), showed a small loss of potency under hypoxic conditions, in contrast to irinotecan which was unaffected by the lower oxygen tension (HCR = 1.12). The effect of **3a** and **4a** in HT29 cells was less effective in oxygen-deprived environment versus normoxic cells, showing more resistance in hypoxic conditions as it happens to the majority of antitumor agents.

Table 6: Growth inhibition of compounds **2a** and **4a** against HT29 colon cancer cells under normoxic and hypoxic conditions

Compound	Normoxia $\text{IC}_{50} \pm \text{SD}$ (μM)	Hypoxia $\text{IC}_{50} \pm \text{SD}$ (μM)	HCR: $\text{IC}_{50 \text{ norm}} / \text{IC}_{50 \text{ hypox}}$
2a	1.73 ± 0.25	7.33 ± 1.60	0.24
4a	1.33 ± 0.22	8.93 ± 1.27	0.15
<i>Irinotecan</i>	3.96 ± 0.66	3.55 ± 0.47	1.12



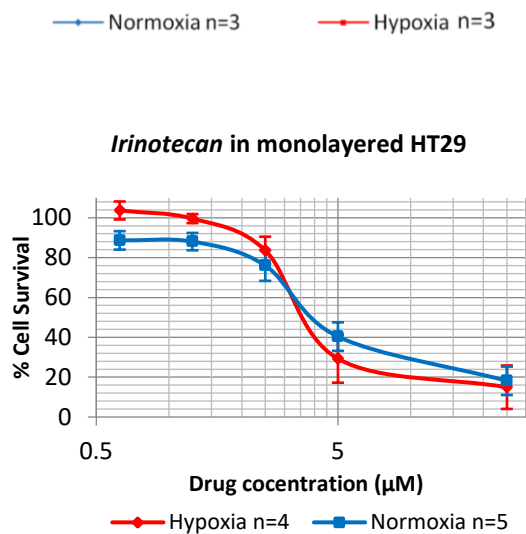


Figure 2: IC₅₀ values and hypoxic cytotoxicity ratio (HCT) for **2a**, **4a** and irinotecan were evaluated under normoxic and hypoxic conditions in adherent HT29 cells using MTT assay. Each value represents the mean of at least three independent experiments

2.2.7. CYP1A1 bioactivation

The natural product ellipticine (**1**) exerts its antiproliferative activity in part via CYP1A1 bioactivation leading to a metabolite capable of covalently binding DNA. CYP1A1 has been shown to be differentially overexpressed in CRC while its expression in normal surrounding epithelia is relatively low [21]. Given scaffold similarity of the lactones presented in this study with ellipticine, interrogation of their potential for CYP1A1 bioactivation were assessed in the CHO/CHO1A1 isogenic cell line pair. Analogue **2a** and the thiofuranone analogue **4a** were chosen as a suitable pair for this investigation. Lactone **2a** was found to be 3.7-fold more antiproliferative in CHO1A1 cells compared with parental CHO cells while the thiofuranone **4a** had much lower potentiation effect in the presence of CYP1A1 (Table 7). Ellipticine was shown to be approximately 15-fold more potent in CHO1A1 cells, which is in accordance with previous studies that have confirmed CYP1A1 as a bioactivating enzyme responsible for generating a metabolite capable of damaging DNA via adduct formation [22].

Table 7. Antiproliferative activity of lactones **2a** and **4a** in mock and CYP1A1-transfected CHO cell lines

Compound	CHO	CHO1A1	PF
2a	1.48±0.1	0.4±0.1	3.7
4a	1.52±0.1	2.6±0.7	0.6
Ellipticine	0.02±0.0	0.0193±0.00	15.6

^aIC₅₀ values for **2a**, **4a** and ellipticine were derived from at least three independent experiments

3. Molecular Modeling Studies

Compound **2a** (L2a) was selected as a representative member of the diverse benzodioxine analogues of the most active series **a** described above for the determination of its most probable binding site to KRas. To achieve this objective, we thoroughly explored the conformational space of the KRas-L2a system performing a docking procedure over the five different predicted binding sites of the KRas protein [23, 24], (Figure 3) as explained in the experimental section. For each binding site, we selected the five best docked poses. Then, the twenty-five complexes were prepared and subjected to 20 ns of molecular dynamics (MD) for an initial analysis. The total binding free energies calculated by both MMPBSA and MMGBSA approaches were plotted as a function of the trajectory length to determine the convergence behavior of the different complexes. Table S1 of Supporting Information contains all the information extracted from the global analysis process.

Visual inspection of the MD trajectories allows us to classify the different complexes in four different groups. The first one corresponds to those systems where the ligand moves away from the protein during the 20 ns of MD (Case [1] and no binding is observed (Table S1 and Figures S7, S8, S9 and S16). The second group corresponds to complexes with bad convergence and low values of ΔG_b (Case [2] in Table S1 and Figures S10, S15 and S17). The third one is composed by those complexes that present good convergence only for the last 5 ns, but with $|\Delta G_b|$ smaller than 25 kcal/mol (Case [3] in Table S1 and Figures S2, S5, S12 and S13). Finally, the last group corresponds to those complexes that present good convergence during more than 5 ns, but with $|\Delta G_b|$ smaller than 25 kcal/mol (Case [4] in Table S1 and Figures S1, S3, S4, S6, S11 and S14). All complexes included in these four groups (Colored red in Table S1) were discarded from future analysis and only the remaining eight complexes

which showed better convergence and $|\Delta G_b|$ values greater than 25 kcal/mol were retained (Yellow, brown and green colors in Table S1).

In a second step, the length of the MD of the eight best complexes was extended to 100 ns to permit a better-induced fit of the protein. In this step, only one structure was rejected because the binding energy for the last 5 ns was worse than -25 kcal/mol (Brown color in Table S1 and Figure S18). Thus, to distinguish between the remaining seven poses the length of the MD was extended to 300 ns. Now, poses 1 and 3 of pocket 1 and poses 1 and 3 of pocket 2 were discarded because of their no-binding or low binding energy (Yellow color in Table S1 and Figures S19 to S22). Finally, for the three remaining poses (Green color in Table S1) the length of the MD was extended to 700 ns. Pose 4 of pocket 1 was clearly stable during the last 300 ns; however, it was discarded because of its worse binding energy as compared to those of the remaining two poses (Figure S23). The two remaining poses present very similar (both PB and GB) final binding energies (Green color in Table S1 and Figures S24 and S25), with both involving docking at pocket P3. However, a visual inspection of the final structures (Figure S26) shows that they are not located in the P3 pocket but inserted between helix α_3 and α_4 , a binding site not previously described until now, with their carbonyl groups pointing in opposite directions. Thus, considering all this information, we can conclude that the most probable binding mode of compound **2a** corresponds to pose 1 of pocket 3, as in this structure the carbonyl group presents a hydrogen bond with the protein that does not appear in the other structure (pose 4 of pocket 3). This finding explains the fact that compounds of series **b**, which share the carbonyl group at the opposite side of the aliphatic moiety, present a very low activity.

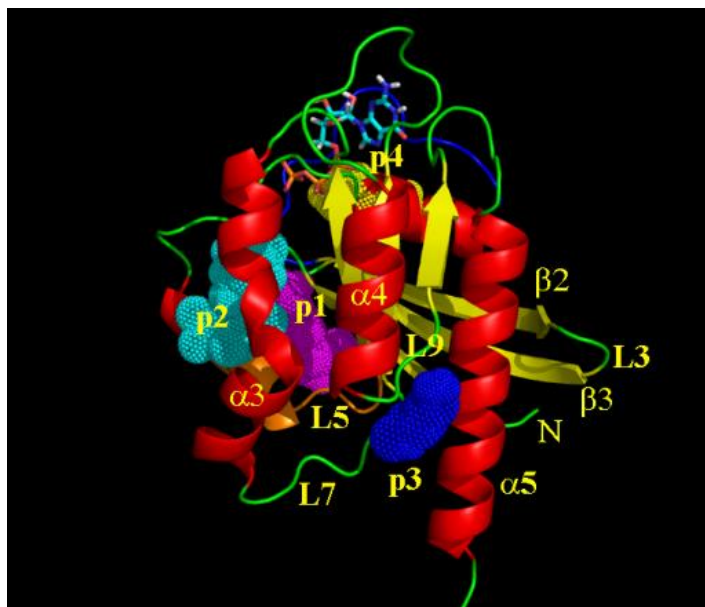


Figure 3. The most relevant structural motifs of the KRas protein are indicated. The location of the four allosteric ligand-binding sites is shown in colored mesh (p1 to p4) and the P3b allosteric site is located between L5, L7 and $\alpha 5$ motifs. The predicted binding site of the studied compound is located between the $\alpha 3$ and $\alpha 4$ helix. The GTP cofactor is represented by sticks

Residues of KRas contributing to the binding free energy of the selected KRas-L2a complex were analyzed during the last 100ns of MD, and the average values are reported in Figure S26. A 3D representation of the binding site and the interacting residues is shown in Figure 3. From this figure, it can be seen that the ligand is inserted in a deeper pocket, where the fused rings interact with the hydrophobic residues Phe90, Glu91, Ile9364, Hie94, Leu133 and Tyr137. In addition, the complex establishes one stable hydrogen bond (HB) with the protein, between the carbonyl oxygen of the ligand and the charged residue Arg97.

Finally, we introduced a methoxy group as a substituent of the first aromatic ring of the tetracyclic lactone (at C-7 position, compound **7a**) to compare its stability with the original **2a** ligand. As expected, both the MMPBSA and MMGBSA approaches suggest that the substituted compound has a smaller binding energy than the original one although the difference is small; 0.8 kcal/mol and 0.2 kcal/mol for the MMGBSA and MMPBSA methods, respectively. The convergence of ΔG_b is shown in figure S28 (supporting information). The final structures of both compounds are displayed in figure S29 (supporting information), in which we can see that the position of the **7a** modified compound is displaced from the original starting point.

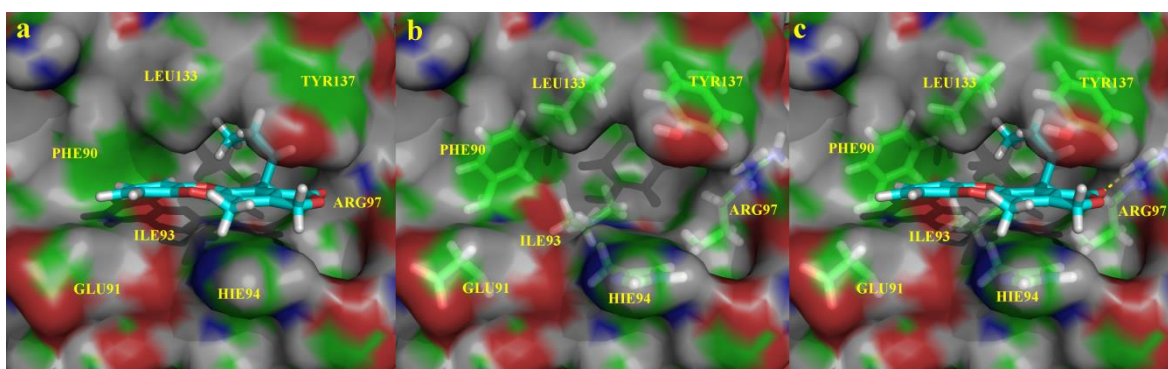


Figure 4. A Spatial representation of the complex KRas-L2a for the selected structure. a) Description of the binding pocket with the ligand. b) Spatial representation of the most important residues that interact with the ligand. c) The KRas-L2a complex showing the hydrogen bonds in green

4. Conclusion

A series of linear 1,4-benzodioxine lactones related to ellipticine were investigated and several compounds were synthesized from 1,4-benzodioxine-2-carboxylic acid in 4 steps. A clear conclusion is that lactones possessing an alkyl chain on the same side as the carbonyl group of the lactone (**2a**, **3a**, **4a**, **5a** and **6a**, series **a**) are more active than the corresponding positional isomers with the alkyl chain on the opposite side of the carbonyl (series **b**). Regarding the length of the alkyl group, in general, the butyl, pentyl and hexyl chains were the best. These tetracyclic lactones of the series **a** have shown an interesting profile of biological activities. It should be noted that the introduction of a methoxyl group into the aromatic ring of lactone **3a** causes a considerable loss of activity (**7a**) as does the introduction of a sulfur atom (**6a**).

Analogue **2a** possessing a butyl side chain exhibited an interesting biological profile. It exhibited activity in the KRas-Wnt synthetic lethal primary single point assay, exhibited both antiangiogenic and antiproliferative properties while potentiation of anticancer effect is possible in the presence of CYP1A1 which is known to be expressed in a number of cancer types including colorectal carcinoma (CRC) [25]. As such, lactone **2a** represents a good starting point for further medicinal chemistry aimed at generating novel agents to probe the colorectal carcinoma microenvironment.

5. EXPERIMENTAL SECTION

5.1. Chemistry

Melting points (mp) were determined on a Gallenkamp-apparatus (MFB-595010M) with interior thermometer using open capillary tubes and are reported after correction. IR spectra were obtained using FTIR Perkin-Elmer 1600 Infrared Spectrophotometer. ^1H and ^{13}C NMR spectra were recorded on a Varian Gemini-300 and 400 MHz (75.5 and 100 MHz respectively for ^{13}C). Chemical shifts are reported in parts per million (ppm) relative to the central peak of the used solvent: CDCl_3 (δ , 7.26 (H) and 77.16 (C)), CD_3OD (δ , 3.31 (H) and 49.45 (C)), DMSO-d_6 (δ , 2.49 (H) and 39.51 (C)) as internal standards. The following abbreviations are used for the proton spectra multiplicities: bs, broad signal, s, singlet, d, doublet, t, triplet, q, quadruplet, m, multiplet. Coupling constants (J) are reported in Hertz (Hz). The reactions were monitored by thin-layer chromatography (TLC) analysis using silica gel (60 F254, Merck) plates and compounds were visualized by UV irradiation. Column chromatography was performed with silica gel 60 (230-400 mesh, 0.040-0.063 mm) and automatic column chromatography was performed with a CombiFlash R_f system with UV-vis (PN 68-5230-008) detector and RediSep R_f 4 and 12 g silica gel column. High-resolution mass spectra (HRMS) were performed on a LC/MSD-TOF (2006) (Agilent technologies) at the University of Barcelona (Serveis Científic-Tècnics UB). All reagents were of high quality or were purified before use. All organic solvents were of analytical grade or were purified by standard procedures before use.

The hydroxyacids (**9a-9e**), lactones (**10a-10e**) and furans (**11a-11e**) have been prepared according to the procedure described previously [5] but operating on a larger scale (6-12 g). The yields obtained are indicated in Scheme 1.

5.1.1. Preparation of lactones (2a-7a and 2b-7b) via Diels-Alder cycloadditions of the furans (11a-e). General procedure. 2(5*H*)-furanone (30 mmol) or 2(5*H*)-thiofuranone (30 mmol) and BF_3 .etherate (catalytic amount) were added to the corresponding diene **11a-11e** (10 mmol) free of solvent at room

temperature. The obtained mixture was then stirred in a hermetically closed flask on a pre-heated bath at 90 °C for 6 h. The crude product was purified with silica gel column chromatography and hexane/ethyl acetate was used as eluent. Two positional isomers were obtained, which were accurately separated and identified.

5.1.1.1. 11-Butyl-4-methyl-1-oxo-3(*H*)-isobenzofuro[5,6-*b*][1,4]benzodioxine (2a). Following the general procedure described above for the preparation of polycyclic lactones and using as starting materials the diene **11a** (3.4 g, 13.9 mmol), and the lactone, the lactone **2a** (1.40 g, 4.43 mmol) was obtained. The crude product was purified by silica gel column chromatography, using hexane/ethyl acetate 97/3 as eluent. The lactone was obtained as a white solid in 33% yield. The isomer **2b** (1.70 g, 5.37 mmol) was obtained in 39% yield, by using the same eluent. Analytical data for **2a**: mp 122-125 °C (hexane/ethyl acetate). IR (KBr) ν (cm⁻¹): 1750 (C=O), 1258 (Ar-O), 1098 (C-O). RMN-¹H (CDCl₃, 200 MHz) δ (ppm): 0.96 (t, *J* = 7.0 Hz, 3H, **CH**₃), 1.25-1.50 (m, 2H, **CH**₂CH₃), 1.51-1.60 (m, 2H, **CH**₂CH₂CH₃), 2.17 (s, 3H, CH₃), 3.05 (t, *J* = 7.0 Hz, 2H, **CH**₂), 5.09 (s, 2H, CH₂O), 6.84-6.90 (m, 4H, Ar). ¹³C NMR (CDCl₃, 75.5 MHz) δ (ppm): 10.7 (CH₃), 13.9 (CH₃), 22.5 (CH₂), 23.2 (CH₂), 32.1 (CH₂), 67.6 (CH₂), 116.3 (CH), 116.5 (CH), 116.6 (C), 117.2 (C), 123.9, and 124.5 (CH), 129.3 (C), 140.7, and 141.0 (C), 141.4, and 142.0 (C), 144.4 (C), 169.0 (C). Anal. Calcd. for C₁₉H₁₈O₄: C 73.53%; H 5.85%. Found: C 73.48%; H 5.91%.

5.1.1.2. 4-Butyl-11-methyl-1-oxo-3(*H*)-isobenzofuro[5,6-*b*][1,4]benzodioxine (2b). mp 153-155 °C (ethyl acetate). IR (KBr) ν (cm⁻¹): 1743 (C=O), 1270 (Ar-O), 1160 (C-O). ¹H NMR (CDCl₃, 200 MHz) δ (ppm): 0.95 (t, *J* = 7.0 Hz, 3H, **CH**₃), 1.25-1.45 (m, 2H, **CH**₂CH₃), 1.45-1.62 (m, 2H, **CH**₂CH₂CH₃), 2.55 (s, 3H, CH₃), 2.57 (t, *J* = 7.0 Hz, 2H, **CH**₂), 5.09 (s, 2H, CH₂O), 6.68-6.95 (m, 4H, Ar). ¹³C NMR (CDCl₃, 75.5 MHz) δ (ppm): 9.39 (CH₃), 13.8 (CH₃), 22.7 (CH₂), 25.5 (CH₂), 31.1 (CH₂), 67.8 (CH₂), 116.4, and 116.3 (CH), 117.8 (C), 121.8 (C), 123.8 (C), 123.9, and 124.4 (CH), 141.3 (C), 141.5 (C), 144.4 (C), 170.7 (C). Anal. Calcd. for C₁₉H₁₈O₄: C 73.53%; H 5.85%. Found: C 73.69%; H 5.89%.

5.1.1.3. 4-Methyl-11-pentyl-1-oxo-3(*H*)-isobenzofuro[5,6-*b*] [1,4]benzodioxine (3a). A mixture of the diene **11b** (3.5 g, 13.6 mmol) and the lactone was treated following the general procedure to prepare lactones as described above. The crude product was purified by silica gel column chromatography, using hexane/ethyl acetate 98/2 as eluent, obtaining the lactone **3a** as a white solid in 30% (1.4 g, 4.0 mmol) yield. The isomer **3b** was obtained in 48% yield (2.18 g, 6.5 mmol) using hexane/ethyl acetate 99/1 as eluent. Analytical data for **3a** mp 108-110 °C (ethyl acetate). IR (KBr) ν (cm⁻¹): 1750 (C=O), 1260 (Ar-O), 1105 (Ar-O). ¹H NMR (CDCl₃, 300 MHz) δ (ppm): 0.83-0.89 (m, 3H, **CH**₃), 1.33-1.45 (m, 4H, (**CH**₂)₂), 1.50-1.65 (m, 2H, **CH**₂), 2.18 (s, 3H, CH₃), 3.05 (t, *J* = 7.5 Hz, 2H, **CH**₂), 5.05 (s, 2H, CH₂O), 6.69-7.02 (m, 4H, Ar). ¹³C NMR (CDCl₃, 75.5 MHz) δ (ppm): 10.8 (CH₃), 14.0 (CH₃), 22.4 (CH₂), 23.3 (CH₂), 29.4 (CH₂), 31.4 (CH₂), 67.5 (CH₂), 116.4 and 116.4 (CH), 116.8 (C), 117.2 (C), 124.0 and 124.8 (CH), 129.3 (C), 140.7 and 141.2 (C), 141.8 and 142.2 (C), 144.9 (C), 170.6 (C). Anal. Calcd. for C₂₀H₂₀O₄: C 74.06%; H 6.21%. Found: 74.31%; H 6.44%.

5.1.1.4. 11-Methyl-4-pentyl-1-oxo-3(*H*)-isobenzofuro[5,6-*b*][1,4]benzodioxine (3b). mp 145-146 °C (ethyl acetate). IR (KBr) ν (cm⁻¹): 1742 (C=O), 1264 (Ar-O), 1140 (Ar-O). ¹H NMR (CDCl₃, 200 MHz) δ (ppm): 0.83-0.99 (m, 3H, **CH**₃), 1.19-1.38 (m, 4H, **CH**₂), 1.42-1.58 (m, 2H, **CH**₂), 2.55 (s, 3H, CH₃), 2.53 (t, *J* = 7.5 Hz, 2H, **CH**₂), 5.07 (s, 2H, CH₂O), 6.60-6.93 (m, 4H, Ar). ¹³C NMR (CDCl₃, 50.3 MHz) δ (ppm): 9.4 (CH₃), 14.0 (CH₃), 22.5 (CH₂), 26.0 (CH₂), 28.5 (CH₂), 31.7 (CH₂), 67.5 (CH₂), 116.2 and 116.5 (CH), 117.5 (C), 121.7 (C), 123.9 (C), 124.0, and 124.4 (CH), 141.3 (C), 141.7 and 141.8 (C), 144.2 (C), 170.9 (C). Ana.l Calcd. for C₂₀H₂₀O₄: C 74.06%; H 6.21%. Found: C 74.32%; H 6.09%.

5.1.1.5. 11-Hexyl-4-methyl-1-oxo-3(*H*)-isobenzofuro[5,6-*b*] [1,4]benzodioxine (4a). The diene **11c** (3.1 g, 11.4 mmol) and the lactone were treated following the general procedure to prepare lactones as described above to obtain lactone **4a**. The crude product was purified by silica gel column chromatography, using hexane/ethyl acetate 98/2 as eluent to obtain the lactone as a white solid in 36%

yield (1.39 g, 4.09 mmol). The isomer **4b** (1.55 g, 4.56 mmol) was obtained in 40% yield using the same eluent. Analytical data for **4a**: mp 131-133 °C (ethyl acetate). IR (KBr) ν (cm⁻¹): 1760 (C=O), 1252 (Ar-O), 1110 (Ar-O). ¹H NMR (CDCl₃, 200 MHz) δ (ppm): 0.82-0.90 (m, 3H, **CH**₃), 1.18-1.42 (m, 6H, **CH**₂)₃), 1.54-1.64 (m, 2H, **CH**₂), 2.14 (s, 3H, CH₃Ar), 3.04 (t, *J* = 7.5 Hz, 2H, **CH**₂), 5.04 (s, 2H, CH₂O), 6.72-7.00 (m, 4H, Ar). ¹³C NMR (CDCl₃, 50.3 MHz) δ (ppm): 10.7 (CH₃), 14.3 (CH₃), 22.7 (CH₂), 23.3 (CH₂), 29.0 (CH₂), 30.0 (CH₂), 31.5 (CH₂), 67.4 (CH₂), 116.0, and 116.3 (CH), 116.6 (C), 117.3 (C), 124.0 and 124.5 (CH), 129.3 (C), 140.7 and 140.8 (C), 141.3 and 142.0 (C), 144.5 (C), 170.7 (C). Anal. Calcd. for C₂₁H₂₂O₄: C 74.54%; H 6.55%. Found: C 74.46%; H 6.62%.

5.1.1.6. 4-Hexyl-11-methyl-1-oxo-3(H)-isobenzofuro[5,6-*b*][1,4]benzodioxine (4b). mp 149-150 °C (ethyl acetate). IR (KBr) ν (cm⁻¹): 1759 (C=O), 1260 (Ar-O), 1135 (Ar-O). ¹H NMR (CDCl₃, 200 MHz) δ (ppm): 0.80-0.89 (m, 3H, **CH**₃), 1.20-1.40 (m, 6H, (**CH**₂)₃), 1.43-1.64 (m, 2H, **CH**₂), 2.43 (s, 3H, CH₃C11), 2.40 (t, *J* = 7.5 Hz, 2H, **CH**₂), 5.10 (s, 2H, CH₂O), 6.81-6.97 (m, 4H, Ar). ¹³C NMR (CDCl₃, 50.3 MHz) δ (ppm): 9.4 (CH₃), 14.2 (CH₃), 22.7 (CH₂), 26.0 (CH₂), 28.9 (CH₂), 29.3 (CH₂), 31.4 (CH₂), 67.4 (CH₂), 116.0 and 116.1 (CH), 117.5 (C), 121.3 (C), 124.0 and 124.3 (CH x 2), 124.1 (C), 141.0 (C x 2), 141.5 (C), 144.3 (C), 170.8 (C). Anal. Calcd. for C₂₁H₂₂O₄: C 74.54%; H 6.55%. Found: C 74.67%; H 6.35%.

5.1.1.7. 4-Methyl-11-(4-bromobutyl)-1-oxo-3(H)-isobenzofuro[5,6-*b*][1,4]benzodioxine (5a). A mixture of the diene **11d** (3.8 g, 11.7 mmol) and the lactone was treated following the general procedure to prepare lactones as described above to obtain **5a**. The crude product was purified by silica gel column chromatography, using hexane/ethyl acetate 90/10 as eluent to obtain the desired lactone **5a** as a white solid in 31% yield (1.43 g, 3.62 mmol). The isomer **5b** (2.08 g, 5.26 mmol) was obtained as a white solid in 43% yield using hexane/ethyl acetate 8/2. mp 146-148 °C (hexane/dichloromethane). IR (KBr) ν (cm⁻¹): 1754 (C=O), 1260 (Ar-O), 1032 (Ar-O), 751 (C-Br). ¹H NMR (CDCl₃, 200 MHz) δ (ppm): 1.64-1.87 (m, 2H, **CH**₂), 1.87-2.03 (m, 2H, **CH**₂), 2.16 (s, 3H, CH₃), 3.08 (t, *J* = 7.4 Hz, 2H, **CH**₂), 3.47 (m,

2H, **CH**₂), 5.05 (s, 2H, CH₂O), 6.87-6.95 (m, 4H, Ar). ¹³C NMR (CDCl₃, 50.3 MHz) δ(ppm): 10.8 (CH₃), 22.3 (CH₂), 28.3 (CH₂), 32.3 (CH₂), 33.7 (CH₂), 67.8 (CH₂), 116.1 and 116.4 (CH), 117.1 and 117.2 (C), 124.1 and 124.6 (CH), 128.0 (C), 140.5 and 140.8 (C), 141.3 and 142.2 (C), 144.8 (C), 170.4 (C). Anal Calcd. for C₁₉H₁₇BrO₄: C 58.63%; H 4.40%, Br 20.53%. Found: C 58.56%; H 4.34%, Br 20.88%.

5.1.1.8. 11-Methyl-4-(4-bromobutyl)-1-oxo-3(*H*)-isobenzofuro[5,6-*b*][1,4]benzodioxine (5b).

Analytical data: mp 160-162 °C (dichloromethane). IR (KBr) ν (cm⁻¹): 1753 (C=O), 1259 (Ar-O), 1025 (C-O), 753 (C-Br). ¹H NMR (CDCl₃, 200 MHz) δ(ppm): 1.64-1.83 (m, 2H, **CH**₂), 1.85-2.04 (m, 2H, **CH**₂), 2.54 (s, 3H, CH₃), 2.59 (t, *J* = 7.4 Hz, 2H, **CH**₂), 3.47 (t, *J* = 6.0 Hz, 2H, **CH**₂Br), 5.10 (s, 2H, CH₂O), 6.87-6.98 (m, 4H, Ar). ¹³C NMR (CDCl₃, 50.3 MHz) δ(ppm): 9.4 (CH₃), 24.8 (CH₃), 27.3 (CH₂), 31.9 (CH₂), 33.1 (CH₂), 67.5 (CH₂), 116.1 and 116.4 (CH), 117.7 (C), 120.3 (C), 122.6 (C), 123.9 and 124.5 (CH), 124.6 (C), 140.7 and 141.0 (C), 141.4 (C), 144.4 (C), 170.8 (C). Anal. Calcd. for C₁₉H₁₇BrO₄: C 58.63%; H 4.40%, Br 20.53%. Found: C 58.77%; H 4.56%, Br 20.77%.

5.1.1.9. 11-Hexyl-4-methyl-1-oxo-3(*H*)-isobenzothiofeno[5,6-*b*][1,4]benzodioxine (6a).

A mixture of the diene **11c** (4 g, 14.7 mmol) and the thiolactone was treated following the general procedure to prepare lactones as described above to obtain **6a**. The crude product was purified by silica gel column chromatography, using as eluent hexane/ethyl acetate 80/20 to obtain the desired lactone as a white solid in 39% yield (2.065 g, 5.73 mmol). The isomer **6b** (2.44 g, 6.76 mmol) was obtained using hexane/ethyl acetate 70/30 as a white solid in 46% yield. mp 126-129 °C (ethyl acetate). IR (KBr) ν (cm⁻¹): 2928 (C-H), 1670 (C=O), 1265 (Ar-O), 1100 (C-O). ¹H NMR (CDCl₃, 200 MHz) δ(ppm): 0.85-0.98 (m, 3H, CH₃), 1.25-1.57 (m, 6H, (**CH**₂)₃), 1.55-1.60 (m, 2H, **CH**₂), 2.21 (s, 3H, CH₃), 3.10 (t, *J* = 7.5 Hz, 2H, **CH**₂), 4.16 (s, 2H, CH₂S), 6.90-6.96 (m, 4H, Ar). ¹³C NMR (CDCl₃, 50.3 MHz) δ(ppm): 10.4 (CH₃), 14.4 (CH₃), 22.9 (CH₂), 23.2 (CH₂), 29.5 (CH₂), 30.1 (CH₂), 32.0 (CH₂), 32.1 (CH₂), 116.3 and 116.4

(CH), 119.6 (C), 123.9 and 124.5 (CH), 127.3 (C), 128.3 (C), 140.0 (C), 141.3 and 141.6 (C), 143.4 (C), 197.0 (C). Anal. Calc. for C₂₁H₂₂O₃S: C 71.16%; H 6.26%. Found: C 70.99%; H 6.45%.

5.1.1.10. 4-Hexyl-11-methyl-1-oxo-3(*H*)-isobenzothiofeno[5,6-*b*][1,4]benzodioxine (6b). Analytical data of **6b**: mp 131-133 °C (ethyl acetate). IR (KBr) ν (cm⁻¹): 2926 (C-H), 1678 (C=O), 1268 (Ar-O). ¹H NMR (CDCl₃, 200 MHz) δ (ppm): 0.86-0.93 (m, 3H, CH₃), 1.21-1.40 (m, 6H, (CH₂)₃), 1.46-1.66 (m, 2H, CH₂), 2.56 (s, 3H, CH₃C11), 2.66 (t, *J* = 7.5 Hz, 2H, CH₂), 4.23 (s, 2H, CH₂S), 6.69-6.98 (m, 4H, Ar). ¹³C NMR (CDCl₃, 50.3 MHz) δ (ppm): 9.8 (CH₃), 14.1 (CH₃), 22.7 (CH₂), 26.0 (CH₂), 29.0 (CH₂), 29.5 (CH₂), 29.8 (CH₂), 31.7 (CH₂), 116.3 and 116.5 (CH), 123.3 (C), 123.8 and 124.5 (CH), 124.6 (C), 128.0 (C), 140.1 and 141.2 (C), 141.7 and 142.8 (C), 143.7 (C), 197.5 (C). Anal. Calcd. for C₂₁H₂₂O₃S: C 71.16%; H 6.26%. Found: C 71.33%; H 6.44%.

5.1.1.11. 4-Methyl-8-methoxy-11-pentyl-1-oxo-3(*H*)-isobenzofuro[5,6-*b*][1,4]benzodioxine (7a). A mixture of the diene **11f** (3.2 g, 11.11 mmol) and the lactone was treated following the general procedure to prepare lactones as described above to obtain **7a**. The crude product was purified by silica gel column chromatography, using hexane/ethyl acetate 99/1 as eluent to obtain the desired lactone as a white solid in 37% of yield (1.523 g, 4.11 mmol). The isomer **7b** (1.98 g, 5.33 mmol) was obtained with hexane/ethyl acetate 98/2 as a white solid in 45% yield. Analytical data for **7a**: mp 137-139 °C (hexane/ethyl acetate). IR (KBr) ν (cm⁻¹): 1754 (C=O), 1260 (Ar-O), 1126 (C-O). ¹H NMR (CDCl₃, 200 MHz) δ (ppm): 0.83-0.88 (m, 3H, CH₃), 1.30-1.41 (m, 4H, (CH₂)₂), 1.47-1.66 (m, 2H, CH₂), 2.15 (s, 3H, CH₃Ar), 3.03 (t, *J* = 7.5 Hz, 2H, CH₂), 3.76 (s, 3H, CH₃O), 5.06 (s, 2H, CH₂O), 6.42-6.48 (m, 2H, C1H, C7H), 6.48 (s, 1H, C9H), 6.78-6.85 (m, 1H, C6H). ¹³C NMR (CDCl₂, 50.3 MHz) δ (ppm): 10.8 (CH₃), 14.2 (CH₃), 22.6 (CH₂), 23.4 (CH₂), 29.8 (CH₂), 31.6 (CH₂), 55.9 (CH₃), 67.7 (CH₂), 102.3 (CH), 108.7 (CH), 116.5 (CH), 116.4 (C), 117.0 (C), 129.2 (C), 134.9 (C), 140.2 (C), 142.0 (C), 142.2 (C), 145.0 (C), 156.2 (C), 170.4 (C). Anal. Calcd. for C₂₂H₂₄O₅: C 71.72%; H 6.57%. Found: C 71.98%; H 6.65%.

5.1.1.12. 11-Methyl-7-methoxy-4-pentyl-1-oxo-3(*H*)-isobenzofuro[5,6-*b*][1,4]benzodioxine (7b).

Analytical data: mp 117-119 °C (ethyl acetate). IR (KBr) ν (cm⁻¹): 1750 (C=O), 1260 (Ar-O), 1030 (C-O). ¹H NMR (CDCl₃, 200 MHz) δ (ppm): 0.80-0.93 (m, 3H, CH₃), 1.20-1.39 (m, 4H, (CH₂)₂), 1.40-1.65 (m, 2H, CH₂), 2.54 (s, 3H, CH₃C11), 2.55 (t, *J* = 7.5 Hz, 2H, CH₂), 3.80 (s, 3H, CH₃O), 5.12 (s, 2H, CH₂O), 6.41-6.52 (m, 1H, C8H), 6.49 (s, 1H, C6H), 6.82-6.85 (m, 1H, C9H). ¹³C NMR (CDCl₃, 50.3 MHz) δ (ppm): 9.5 (CH₃), 14.1 (CH₃), 22.3 (CH₂), 26.0 (CH₂), 28.4 (CH₂), 31.5 (CH₂), 55.9 (CH₃), 67.7 (CH₂), 102.4 (CH), 108.9 (CH), 116.4 (CH), 117.9 (C), 121.6 (C), 124.2 (C), 135.5 (C), 141.3, 141.4, and 141.5 (C), 144.0 (C), 155.9 (C), 171.1 (C). Anal. Calcd. for C₂₁H₂₂O₅: C 71.17%; H 6.26%. Found: C 71.87%; H 6.35%.

5.2. Biological Experimental

5.2.1. L1210 Inhibition Growth Rate Determination. L1210 leukemia cells were grown in RPMI 1640 medium, supplemented with 2 mM of L-glutamine, 200 IU/mL of penicillin, 50 μ g/mL of streptomycin and 20% heat inactivated horse serum. They were incubated at 37 °C in a 5% CO₂ atmosphere. The tested compounds studied were dissolved in DMSO (0.5% of final incubation volume) and added to the exponential growth phase cells seeded at an initial concentration of 0.8 x 10⁵ cells/mL. After 48 h, the cells were counted in triplicate using a Coultronics Coulter Counter and the results were expressed as the compound concentration, which inhibited cell growth by 50% as compared to the control (IC₅₀). The IC₅₀ values were calculated from regression lines obtained from the probit of the percent cell growth inhibition plotted as a function of the logarithm of the dose.

5.2.2. Inhibition of Cellular Proliferation and Cell Cycle Effects [26]. L1210 leukemia cells were grown in RPMI 1640 medium supplemented with 2 mM of L-glutamine, 200 IU/mL of penicillium, 50 μ g/mL of streptomycin, and 20% heat inactivated horse serum. The cells were incubated for 21 h at 37

°C in a 5% CO₂ atmosphere and incubated with an appropriate compound concentration range. Cells were then fixed by ethanol (70% v/v), then washed, and incubated with PBS containing 100 μM of RNase and 25 μM/mL of propidium iodide for 30 min at room temperature. For each concentration, 10⁴ cells were analyzed using a flow cytometer (Beckman Coulter). Results were expressed as a percentage of cells accumulated in each phase of the cell cycle and are indicated.

5.2.3. Cell culture [26]. HT29 human colorectal adenocarcinoma cells were cultured in 10 mL RPMI 1640 medium supplemented with fetal bovine serum, L-glutamine and sodium pyruvate. Cells were maintained at 37 °C in a humidified atmosphere of 95% air and 5% CO₂, or under hypoxic conditions (0.1% O₂, 94.9% N₂, 5% CO₂) in a Whitley H35 Hypoxia-station (Don Whitley Scientific, Shipley, UK).

In addition, seeded into 96-well plates at a density of 1.8 x 10³ cells per well for chemosensitivity studies. Next day, compounds were added to the cells in an appropriate concentration and incubated for 24 hours. After this, media was removed and cells were washed once with 100 μL of PBS and replaced with 200 μL of fresh medium. In case of the hypoxic investigations both PBS and medium were incubated at least 24 hours under hypoxic conditions to ensure appropriate O₂ level was reached all cytotoxic drug stock solutions were prepared in DMSO, fractioned and stored at -20 °C. Drug concentrations were prepared with complete RPMI immediately before use and the final concentration of DMSO did not exceed 0.1% (v/v). Chemosensitivity was carried out using the MTT assay as previously described (5.2.1).

5.2.4. OIDD Lilly Tests

KRas inhibition studies and antiangiogenesis activities (performed at Lilly) were performed as described in the procedures indicated in the OIDD-Lilly program (Open Innovation Drug Discovery, Eli Lilly) (<https://openinnovation.lilly.com>).

5.3. Molecular modeling methods

Calculations were obtained with the AMBER v.14 software package [27] using the PMEMD program (CPU and GPU versions). The ff14SB [28] force field was used for the protein and the gaff [29] one for the ligand. Force field parameters for GTP were obtained from Meagher et al [30] and the 3D structure of the Kras protein was obtained from the Protein Data Bank server (PDB) with ID code 4DSN [31]. Bond orders and protonation states of the protein were automatically adjusted by using the protein preparation wizard workflow included in the Maestro v.10.0 software package [32]. The phosphomethylphosphonic acid guanylate ester (GCP) cofactor was manually modified to be transformed into the guanosine triphosphate cofactor (GTP).

5.3.1. Docking of Compound 2a (L2a)

The docking of compound **2a** (L2a) was done using Schrodinger's Glide software [33] with the standard-precision (SP) docking mode. The ligand was prepared with the The LigPrep module of Maestro with default options, and a flexible ligand sampling was done. The same process was repeated for the five pockets identified in ref. [23]. Figure 3 shows pockets one to four, while pocket p3a is located between loops L5 and L7 and helix $\alpha 5$, very close to pocket p3. The five best docked poses for each pocket ranked by the GlideScore energy function were saved for further studies [34].

5.3.2. Study of Compound 2a-OCH₃

Starting from the last snapshot of the L2a molecular dynamics trajectory, a methoxy group was introduced manually as a substituent of the first aromatic ring of the tetracyclic lactone (at C-7 position) to compare its stability with respect to the original **2a** ligand. Next, 100 ns of molecular dynamics were conducted keeping the ligand structure fixed in order to adapt the protein to the new ligand. Then, 900 ns with no restraints were done in order to achieve convergence along the time in the ΔG_b values. To

have the same molecular dynamics length for both compounds, the molecular dynamics of the L2a system was also extended to 900 ns.

5.3.3. Molecular dynamics (MD) simulations

All the KRas-L2a complexes were prepared using the same protocol. The LEaP module of AmberTools v.16 [35] was used to create a cubic box of TIP3P [36] waters with a minimum distance between any atom of the system and the edge of the box of 15 Å and removing water molecules closer than 2.2 Å to any of the complex atoms. Next, the system was neutralized with counterions following a grid-shaped procedure for mapping electrostatic potential surface. Finally, the ParmEd program was used to produce hydrogen mass repartitioning to allow an integration time of 4 fs [37]. The prepared structures were heated to 300 K during 200 ps at a constant rate of 30 K/20 ps with harmonic restrains of 1 kcal mol⁻¹ Å⁻² in the protein main atoms. Next, 400 ps at constant pressure were performed to increase the system density using harmonic restrains of 1 kcal mol⁻¹ Å⁻² in the protein main atoms. Finally, different production molecular dynamic simulations were done under the canonical ensemble using a Langevin [38] thermostat with a collision frequency of 3 ps⁻¹ for temperature control. Long-range electrostatic energy was computed using the Particle Mesh Ewald summation method [39] with a cutoff of 9 Å for non-bonded interactions. SHAKE algorithm [40] was used to constrain the bonds involving the hydrogen atoms.

5.3.4. MMPB/GBSA Calculations

The binding free energy, ΔG_{bind} , for all the studied protein-ligand systems was evaluated using the MMGB/PBSA (molecular mechanics generalized Born/ Poisson Boltzmann surface area) methods as

implemented in the MMPBSA.py module of Ambertools v.16 [35]. In this approach, the total binding free energy is calculated as $\Delta G_{\text{binding}} = \Delta H_{\text{gas}}^0 - T\Delta S^0 + \Delta G_{\text{solv}}$, where ΔH_{gas}^0 , the gas phase interaction energy, is calculated as the sum of the internal energy (ΔH_{int}^0) and two non-bonded terms corresponding to the van der Waals (ΔH_{vdW}^0) and electrostatic (ΔH_{elec}^0) molecular mechanics energies: $\Delta H_{\text{gas}}^0 = \Delta H_{\text{int}}^0 + \Delta H_{\text{vdW}}^0 + \Delta H_{\text{elec}}^0$. The solvation free energy (ΔG_{solv}) is obtained by summing the polar (ΔG_{polar}) and nonpolar ($\Delta G_{\text{nonpolar}}$) terms: $\Delta G_{\text{solv}} = \Delta G_{\text{polar}} + \Delta G_{\text{nonpolar}}$. For the MMGBSA method the ΔG_{polar} is calculated using the Onufriev-Bashford-Case (OBC) generalized Born [41] (igb=2) whereas the nonpolar contribution ($\Delta G_{\text{nonpolar}}$) is calculated from the solvent accessible surface area (SASA) according to the equation: $\Delta G_{\text{nonpolar}} = \gamma \text{SASA} + \beta$ where the values for γ and β were set to $0.0072 \text{ kcal mol}^{-1} \text{ \AA}^{-2}$ and 0 kcal mol^{-1} [42]. On the other hand, for the MMPBSA method the ΔG_{polar} is calculated using the Poisson Boltzmann approach while the nonpolar contribution ($\Delta G_{\text{nonpolar}}$) is obtained using $\gamma = 0.00542 \text{ kcal mol}^{-1} \text{ \AA}^{-2}$ and $\beta = 0.92 \text{ kcal mol}^{-1}$ [43]. In both methods, values for interior and exterior dielectric constants were set to 1 and 80, respectively. In order to assess the convergence and stability of the ΔG_{bind} values along the time, MMPB/GBSA computations were performed for the complete MD simulations using 100 structures each nanosecond, extracted each 10 ps, using the cpptraj program as implemented in Ambertools v.16 [35]. The contribution of each KRas residue to the total binding free energy was obtained using the MMGBSA decomposition method [44].

Supporting Information Available: (see footnote on the first page of this article): Additional Molecular studies data of new compounds. This material is available free of charge via the internet at <http://dx.doi.org/ejmech>

Acknowledgements

OIDD screening data supplied courtesy of Eli Lilly and Company—used with Lilly's permission. The Spanish Minister (CTQ2011-29285-C02-02) and the SGR(2014)-1017 Generalitat de Catalunya and the Laboratories Servier (France) are gratefully acknowledged for their financial support.

Author Information

Corresponding Author:

*Address correspondence to: Maria Dolors Pujol· Av. Diagonal 643, 08028-Barcelona, Spain. Phone, +34-93-4024534; fax, +34-93-4035941. E-mail: mdpujol@ub.edu

References and notes

- [1] a) C. Asche, M. Demeunynck, Antitumor carbazoles. *Anticancer Agents Med. Chem.* 2007, 7, 247-267. b) S. Goodwin, A. F. Smith, E. C. Horning, Alkaloids of *Ochrosia elliptica Labill*, *J. Am. Chem. Soc.* 81 (1959) 1903-1908.
- [2] a) Y. S. Tsizin, *Chem. Heterocycl. Compd.* 14 (1978) 925-940. b) P. D. Bass, D. A. Gubler, T. C. Judd, R. M. Williams, *Chem. Rev.* 113 (2013) 6816-6863.
- [3] a) E. G. Russell, E. C. Jianfeng Guo, C. O'Sullivan, M. O'Driscoll, F. O. McCarthy, T. G. Cotter, *Invest New Drugs* 34 (2016) 15–23, b) E. C. O'Sullivan, C. M. Miller, F. M. Deane, F. O. McCarthy, Emerging targets in the bioactivity of ellipticines and derivatives. *Studies in natural products chemistry*, Amsterdam, Netherlands: Elsevier Science Publishers, 6 (2012) 189–226, c) F. M. Deane, E. C. O'Sullivan, A. R. Maguire, J. Gilbert, J. A. Sakoff, A. McCluskey, F. O. McCarthy, Synthesis and evaluation of novel ellipticines as potential anti-cancer agents, *Org. Biomol. Chem.* 11 (2013) 1334-1344, d) C. Auclair, C. Paoletti, Bioactivation of the antitumor drugs 9- hydroxyellipticine and derivatives by a peroxidase-hydrogen peroxide system, *J. Med. Chem.* 24 (1981) 289-295, e) J. Y. Kim, S. G. Lee, J. Y. Chung, Y. J. Kim, J. E. Park, H. Koh, M. S. Han, Y. C. Park, Y. H. Yoo, J. M. Kim, Ellipticine induces apoptosis in human endometrial cancer cells: the potential involvement of reactive oxygen species and mitogen-activated protein kinases, *Toxicology* 289 (2011) 91-102, f) M. Hägg, M. Berndtsson, A. Mandic, R. Zhou, M. C. Shoshan, S. Linder, Induction of endoplasmic reticulum stress by ellipticine plant alkaloids, *Mol. Cancer Ther.* 3 (2004) 489–497, g) X. Jin, D. R. Gossett, S. Wang, D. Yang, Y. Cao, J. Chen, R. Guo, R. K. Reynolds, J. Lin, Inhibition of AKT survival pathway by a small molecule inhibitor in human endometrial cancer cells, *Br. J. Cancer* 91 (2004) 1808-1812.
- [4] a) C. Bozzo, M. D. Pujol, Deoxygenation of 5,12-Epoxy-5,12-dihydro-5,12-dimethyl-1,4-benzodioxino[2,3-g]isoquinoline with Iron Compounds. *Synthesis of Antitumour Agents*, Synlett 2000 550-552, b) C. Bozzo, M. D. Pujol, A short synthesis for the preparation of polycyclic systems containing pyridine ring by Diels-Alder reaction, *Heterocyclic Commun.* 2 (1996) 163-167, c) C. Bozzo, M. D. Pujol, Preparation of methylfuro[3,4-*b*][1,4]benzodioxinones as intermediates for the synthesis of substituted polycyclic systems. Importance of the acid used as catalyst, *Tetrahedron* 55 (1999) 11843-11852, d) C. Bozzo, N. Mur, P. Constans, M. D. Pujol, Furo[3,4-*b*]benzodioxin Cycloadditions a One-Pot Synthesis of Functionalized *Bis*-Adducts, *Eur. J. Med. Chem.* 13 (2009) 2174-2178.

- [5] M. Romero, P. Renard, D.-H. Caignard, G. Atassi, X. Solans, P. Constans, C. Bailly, M. D. Pujol, Synthesis and Structure–Activity Relationships of New Benzodioxinic Lactones as Potential Anticancer Drugs, *J. Med. Chem.* 50 (2007) 294-307.
- [6] <https://openinnovation.lilly.com>
- [7] a) D. A. Chan, A. J. Giaccia, Harnessing synthetic lethal interactions in anticancer drug discovery, *Nat. Rev. Drug Discov.* 10 (2011) 351-364, b) K. Knickelbein, L. Zhang, Mutant KRAS as a critical determinant of the therapeutic response of colorectal cancer, *Genes Dis.* 2 (2015) 4-12, c) J. P. Morris, S. C. Wang, M. Hebrok, KRAS, Hedgehog, Wnt and the twisted developmental biology of pancreatic ductal adenocarcinoma, *Nat Rev Cancer* 10 (2010) 683-695.
- [8] T. L. Riss, R. L. Moravec, A. L. Niles, S. Duellman, H. A. Benink, T. J. Worzella, L. Minor, *Cell Viability Assays*, 2016.
- [9] D. Hanahan, R. A. Weinberg, Hallmarks of cancer: the next generation, *Cell* 144 (2011) 646-674.
- [10] D. Lu, Dan Lu, J. Shen, M. D. Vil, H. Zhang, X. Jimenez, P. Bohlen, L. Witte, Z. Zhu, Tailoring in vitro selection for a picomolar affinity human antibody directed against vascular endothelial growth factor receptor 2 for enhanced neutralizing activity, *J. Biol. Chem.* 278 (2003) 43496-43507.
- [11] J. D. Schwartz, E. K. Rowinsky, H. Youssoufian, B. Pytowski, Y. Wu, Vascular Endothelial Growth Factor Receptor-1 in Human Cancer, *Cancer* 116 (2010) 1027-1032.
- [12] K. M. Cook, W. D. Figg, Angiogenesis inhibitors: current strategies and future prospects, *Cancer J. Clin.* 60 (2010) 222-243.
- [13] D. M. DeMarini, S. Cros, C. Paoletti, P. Lecointe, A. W. Hsie, Mutagenicity and Cytotoxicity of Five Antitumor Ellipticines in Mammalian Cells and Their Structure-Activity Relationships in *Salmonella*, *Cancer Res.* 43 (1983) 3544-3552.
- [14] a) Y. Chen, B. A. Alman, Wnt pathway, an essential role in bone regeneration, *J. Cell. Biochem.* 106 (2009) 353-362. b) S. M. Murphy, M. Kiely, P. M. Jakeman, P. A. Kiely, B. P. Carson, Optimization of an in vitro bioassay to monitor growth and formation of myotubes in real time, *Biosci. Rep.* 36 (2016) e00330 / doi 10.1042/BSR20160036. Open access.
- [15] OIDD Lilly Program. J. A. Lee, P. Shinn, S. Jaken, S. Oliver, F. S. Willard, S. Heidler, R. B. Peery, J. Oler, S. Chu, N. Southall, T. S. Dexheimer, J. Smallwood, R. Huang, R. Guha, A. Jadhav, K. Cox, C. P. Austin, A. Simeonov, G. S. Sittampalam, S. Husain, N. Franklin, D. J. Wild, J. J. Yang, J. J. Sutherland, C. J. Thomas. Novel Phenotypic Outcomes Identified for a Public Collection of Approved Drugs from a Publicly Accessible Panel of Assays, *PLOS one* 2015 1-21.
- [16] G. Amico, L. Basile, G. Romeo, L. Salerno, M. N. Modica, M. A. Siracusa, A. Marrazzo, V. Pittalà, S. Guccione, Rescuing abandoned molecules as Nav1.7 and PCSK9 inhibitors, *J. Adv. Med. Pharmac. Sci.* 5 (2016) 1-10.
- [17] A. I. Minchinton, I. F. Tannock, Drug penetration in solid tumors, *Nat. Rev. Cancer* 6 (2006) 583-592.

- [18] W. A. Denny, The role of hypoxia-activated prodrugs in cancer therapy, *Lancet Oncol.* 1 (2000) 25-29.
- [19] X. Liu; E. M. Weaver; A. B. Hummon, Spectral analysis: Software for the masses, *Anal. Chem.* 85 (2013) 6295-6302.
- [20] W. Y. Ho; S. K. Yeap; C. L. Ho; R. A. Rahim; N. B. Alitheen, Development of multicellular tumor spheroid (MCTS) culture from breast cancer cell and a high throughput screening method using the MTT assay, *PLOS ONE* 7 (2012), e44640.
- [21] D. C. Spink, B. C. Spink, J. Q. Cao, J. A. DePasquale, B. T. Pentecost, M. J. Fasco, Y. Li, T. R. Sutter, Differential expression of CYP1A1 and CYP1B1 in human breast epithelial cells and breast tumor cells, *Carcinogenesis* 19 (1998) 291-298.
- [22] M. Moretti, M. Dell'Omo, M. Villarini, R. Pastorelli, G. Muzi, L. Airoidi, R. Pasquini. Primary DNA damage and genetic polymorphisms for CYP1A1, EPHX and GSTM1 in workers at a graphite electrode manufacturing plant, *BMC Public Health* 7 (2007) 270-280.
- [23] B. J. Grant, S. Lukman, H. J. Hocker, J. Sayyah, J. H. Brown, J. A. McCammon, A. A. Gorfe, Novel Allosteric Site on Ras for Lead Generation, *PLoS One* 2011 6,e25711.A.S.
- [24] S. Capilla, R. Soucek, L. Grau, M. Romero, J. Rubio-Martinez, D. H. Caignard, M. D. Pujol, Substituted tetrahydroisoquinolines: synthesis, characterization, antitumor activity and other biological properties, *Eur. J. Med. Chem.* 145 (2018) 51-63.
- [25] H. M. Sheldrake, S. Travica, I. Johansson, P. M. Loadman, M. Sutherland, L. Elsalem, N. Illingworth, A. J. Cresswell, T. Reuillon, S. D. Shnyder, S. Mkrtchian, M. Searcey, M. Ingelman-Sundberg, L. H. Patterson, K. Pors, Re-engineering of the Duocarmycin Structural Architecture Enables Bioprecursor Development Targeting CYP1A1 and CYP2W1 for Biological Activity, *J. Med. Chem.* 56 (2013) 6273-6277.
- [26] T. Mosmann, Rapid colorimetric assay for cellular growth and survival: application to proliferation and cytotoxicity assays, *J. Immunol. Met.* 65 (1983) 55-63.
- [27] D. Case, V. Babin, J. Berryman, R. Betz, Q. Cai, D. Cerutti, T. E. Cheatham, T. Darden, R. Duke, H. Gohlke, A. Goetz, S. Gusarov, N. Homeyer, P. Janowski, J. Kaus, I. Kolossvary, A. Kovalenko, T. Lee, S. LeGrand, T. Luchko, R. Luo, B. Madej, K. Merz, F. Paesani, D. Roe, A. Roitberg, C. Sagui, R. Salomon-Ferrer, G. Seabra, C. Simmerling, W. Smith, J. Swails, R. Walker, J. Wang, R. Wolf, X. Wu, P. Kollman, *AMBER 14*, 2014; University of California, San Francisco. Maier,
- [28] J. A. Meier, C. Martinez, K. Kasavajhala, L. Wickstrom, K. E. Hauser, C. Simmerling, ff14SB: Improving the Accuracy of Protein Side Chain and Backbone Parameters from ff99SB, *J. Chem. Theory Comput.* 11 (2015) 3696-3713.
- [29] J. Wang, R. M. Wolf, J. W. Caldwell, P. A. Kollman, D. A. Case, Development and testing of a general amber force field, *J. Comput. Chem.* 25 (2004) 1157-1174.

- [30] K. L. Meagher, L. T. Redman, H. A. Carlson, Development of polyphosphate parameters for use with the AMBER force field, *J. Comput. Chem.* 24 (2003) 1016-1025.
- [31] T. Maurera, L. S. Garrenton, A. Oh, K. Pitts, D. J. Anderson, N. J. Skelton, B. P. Fauber, B. Pan, S. Malek, D. Stokoe, M. J. C. Ludlam, K. K. Bowman, J. Wu, A. M. Giannetti, M. A. Starovasnik, I. Mellman, P. K. Jackson, J. Rudolph, W. Wang, G. Fang, Small-molecule ligands bind to a distinct pocket in Ras and inhibit SOS-mediated nucleotide exchange activity, *PNAS* 109 (2012) 5299-5304.
- [32] Schrödinger Release 2016-2: Maestro, Schrödinger, LLC, New York, NY, 2016.
- [33] Schrödinger Release 2016-2: Glide, Schrödinger, LLC, New York, NY, 2016.
- [34] J. J. Pérez, M. S. Tomas, J. Rubio-Martinez, Assessment of the Sampling Performance of Multiple-Copy Dynamics versus a Unique Trajectory, *J. Chem. Inform. Model.* 30 (2016) 1950-1962.
- [35] D. Case, R. Betz, W. Botello-Smith, D. S. Cerutti, T. E. Cheatham, T. Darden, R. E. Duke, T. J. Giese, H. Gohlke, A. Goetz, N. Homeyer, S. Izadi, P. Janowski, J. Kaus, A. Kovalenko, T. Lee, S. LeGrand, P. Li, C. Lin, T. Luchko, R. Luo, B. Madej, D. Mermelstein, K. Merz, G. Monard, H. Nguyen, H. T. Nguyen, I. Omelyan, A. Onufriev, D. R. Roe, A. Roitberg, C. Sagui, C. Simmerling, J. Swails, R. C. Walker, J. Wang, R. M. Wolf, X. Wu, L. Xiao, D. M. York, P. Kollman, *AMBER 2016*. University of California, San Francisco.
- [36] W. L. Jorgensen, J. Chandrasekhar, J. D. Madura, R. W. Impey, M. L. Klein, Comparison of simple potential functions for simulating liquid water. *J. Chem. Phys.* 79 (1983) 926-935.
- [37] C. Hopkins, S. Le Grand, R. Walker, A. Roitberg, A. Long-Time-Step Molecular Dynamics through Hydrogen Mass Repartitioning, *J. Chem. Theory Comput.* 11 (2015) 1864–1874.
- [38] B.P. Uberuaga, M. Anghel, A. F. Voter, Synchronization of trajectories in canonical molecular-dynamics simulations: observation, explanation, and exploitation, *J. Chem. Phys.* **2004**, 120, 6363–6374.
- [39] T. Darden, D. York, L. Pedersen, Particle Mesh Ewald: An N.Log(N) Method for Ewald Sums in Large Systems, *J. Chem. Phys.* 98 (1993) 10089-10092.
- [40] J. P. Ryckaert, G. Ciccotti, H. J. C. Berendsen, Numerical Integration of the Cartesian Equations of Motion of a System with Constraints: Molecular Dynamics of n-alkanes, *J. Comput. Phys.* 23 (1977) 327-341.
- [41] A. Onufriev, D. Bashford, D. A. Case, Exploring protein native states and largescale conformational changes with a modified generalized born model, *Protein Struct. Funct. Bioinf.* 55 (2004) 383–394.
- [42] H. Gohlke, D. A. Case, Converging free energy estimates: MMPB(GB)SA studies on the protein-protein complex Ras-Raf. *J. Comput. Chem.* 25 (2004), 238-250.
- [43] B. Kuhn, P. Gerber, T. Schulz-Gasch, M. Stahl, Validation and use of the MM-PBSA approach for drug discovery, *J. Med. Chem.* 48 (2005) 4040-4048.

[44] H. Gohlke, C. Kiel, D. A. Case, Insights into protein-protein binding by binding free energy calculation and free energy decomposition for the Ras-Raf and Ras-RalGDS complexes, *J. Mol. Biol.* 330 (2003) 891-891.